Korean Chem. Eng. Res., 57(2), 259-266 (2019)
https://doi.org/10.9713/kcer.2019.57.2.259
PISSN 0304-128X, EISSN 2233-9558

Tuning of Electro-optical Properties of Nano-structured SnO_2:Ga Powders in a Micro Drop Fluidized Reactor

Dae Ho Lim*, Si Woo Yang, Dong June Yoo**, Chan Gi Lee*** and Yong Kang**,†**

**Greenhouse Gas Laboratory, Korea Institute of Energy Research, Daejeon, 34129, Korea*
***Department of Chemical Engineering, Chungnam National University, Daejeon, 34134, Korea*
****Advanced Materials & Processing Center, Institute for Advanced Engineering, Yongin, 17180, Korea*
(Received 28 January 2019; Received in revised form 4 March 2019; accepted 5 March 2019)

Abstract – Tuning of electro-optical properties of nano-structured SnO_2:Ga powders in a micro drop fluidized reactor (MDFR) was highly effective to enhance the activities of powders to be used as sensor materials. The tuning was conducted continuously in a facile one-step process during the formation of powders. The microscopic hydrodynamic forces affected the band gap structure and charge transfer of SnO_2:Ga powders through the oxygen and interfacial tin vacancies by providing plausible pyro-hydraulic conditions, which resulted in the decrease in the electrical resistance of the materials. The analyses of room-temperature photoluminescence (PL) spectra and FT-IR exhibited that the tuning could improve the surface activities of SnO_2:Ga powders by adjusting the excitation as well as separation of electrons and holes, thus maximizing the oxygen vacancies at the surface of the powders. The scheme of photocatalytic mechanism of SnO_2:Ga powders was also discussed.

Key words: SnO_2:Ga powder, One-step continuous process, Pyro-hydraulic reaction, Fluidized reactor, Chemical sensing

1. Introduction

Tin oxides (SnO_2) have been regarded as materials to be developed as chemical sensing materials, due to their inherent characteristics including high electron mobility and transparent conductance, wide band gap structure and chemical stability. Those advantages of SnO_2 allow them to be applied in the fields of various kinds of light cells, gas sensors, batteries, electrodes, magnetic semiconductors, etc [1-13].

Since the doping of foreign components into the host materials has been simple but impactive to improve the qualities to reveal the unique functions of host materials, various kinds of ions have been doped into SnO_2 to develop and explore the specific functions of SnO_2 based materials [14-39]. Several methods, including hydrothermal, sol-gel, precipitation, chemical vapor deposition, spray pyrolysis and electrospinning method, have been utilized for the doping of foreign components into SnO_2 and preparation of SnO_2 based materials [25-41]. It has been understood that the optical, electronic, chemical and physical characteristics of the final products are directly related to the methods of doping as well as preparation, since the surface facet, crystallite structure, chemical bonding and electron distribution have been adjusted and determined by means of atomic and electronic behaviors of components during the formation and doping.

For practical applications, however, the doping and preparation method should be continuous in order to make a compromise with the batch modes, which are taking a long time, requiring additional steps such as calcination, annealing, washing or drying and preparing only small amount of product. Spray pyrolysis has been successfully utilized to prepare various kinds of advanced functional powder materials with uniform size and composition continuously [42-46]. However, a more effective method has been required to meet the needs of creation for the more specific and special functions of SnO_2 based advanced materials, which could be possible by controlling the operation conditions during the very short powder formation reaction. In addition, the method should be economic in order to be a process, which can be facilely employed in many fields of industries. To solve those practical demands, a micro drop fluidized reactor (MDFR) was developed, since it can realize the continuous preparation of nanostructured powders with uniform size and composition by means of a one-step process with reasonable production efficiency in a short time [47-52].

A micro drop fluidized reactor was employed in the present study to prepare the Ga doped SnO_2 (SnO_2:Ga) nanostructured powders in a one-step and continuous process with plausible production efficiency. The doping of Ga^{3+} ions was conducted to modify the SnO_2 surface to enhance the gas sensing abilities. Because the Ga^{3+} ion can be a better choice, since its radius (0.062 nm) is more similar to that of Sn^{4+} (0.069 nm) than those of other Group III elements [53], which would compromise the reduction of lattice deformation. The mechanism of sensing reaction of ethanol at the active sites of SnO_2:Ga was examined by considering the excitation and separation of electron-hole pairs at the surface of the powders.

† To whom correspondence should be addressed.
E-mail: kangyong@cnu.ac.kr
‡This article is dedicated to Prof. Yong Kang on the occasion of his retirement from Chungnam National University.

2. Experiments

Ga^{3+} doped SnO_2 nano-structured powders were prepared continuously with reasonable production efficiency by using an MDFR system. The reactor system was composed of micro drop generating, powder formation reaction, micro bubble generating and powder collection parts, as shown in Fig. 1 [48-51]. The micro drops of precursor solutions, which were generated in an atomizing chamber with four oscillators (1.7 MHz, Htech Green Tech.), were transported to the top of the vertical reaction zone by a carrier gas continuously. The reaction zone, which was made of quartz tube (0.03 m ID × 1.2 m in height), was heated by electric furnace to be maintained at 800 °C. The micro drops were fluidized during the reaction by means of micro bubbles generated by a micro bubble generator with a micro flow controller (MFC) and injected into the bottom of the reactor. The flow rates of micro drops and bubbles were 4.0 L/min and 0.4 L/min, respectively, to adjust the favorable reaction conditions [48-51]. As-prepared powders of SnO_2 and SnO_2:Ga were collected by using a thimble filter (ADVANTEC, grade 84).

Diluted solution of $SnCl_4 \cdot 5H_2O$ (Sigma Aldrich 98%) in ethyl alcohol was used as the Sn source and diluted $GaCl_3$ (Alfa Aesar 99.9%) in de-ionized water as the Ga source, respectively, which were mixed sufficiently before atomizing. The atomic ratio of Ga/Sn was in the range of 0~3.0 at.%. The crystalline structure of as-prepared powders was confirmed by analyzing the X-ray diffraction patterns (XRD, MAX-2200 Ultima). The light absorption ability of each sample was analyzed by diffuse reflectance spectra (DRS, Solidspec-3700) using an UV-VIS-NIR spectrophotometer (Shimadzu, UV-3101PC). The shapes and surface morphologies of samples were characterized by using a field-emission scanning electron microscope (FE-SEM, JSM-7000F). To analyze the room-temperature photoluminescence (PL) of samples, a Fluorolog 3 photoluminescence spectrometer (HJY, Japan) was used. The BET surface area and pore size distribution of each sample were determined from the nitrogen adsorption - desorption isotherms (ASAP2010, Micromeritics Ins. Corp.). The chemical compositions of the samples were checked by Fourier transform infrared (FT-IR) spectroscope (Nicolet 6700). The electrical resistivity of each sample, which was fabricated on the alumina substrate equipped with a pair of Pt electrodes, was measured by using an electrometer system. The sensing response was determined by means of the ratio of Ra and Re, which are the resistances in the air and in the ethanol vapor, respectively. The adsorption and recovery times were determined as the times taken by the sensing system to achieve 90% of the total resistance change.

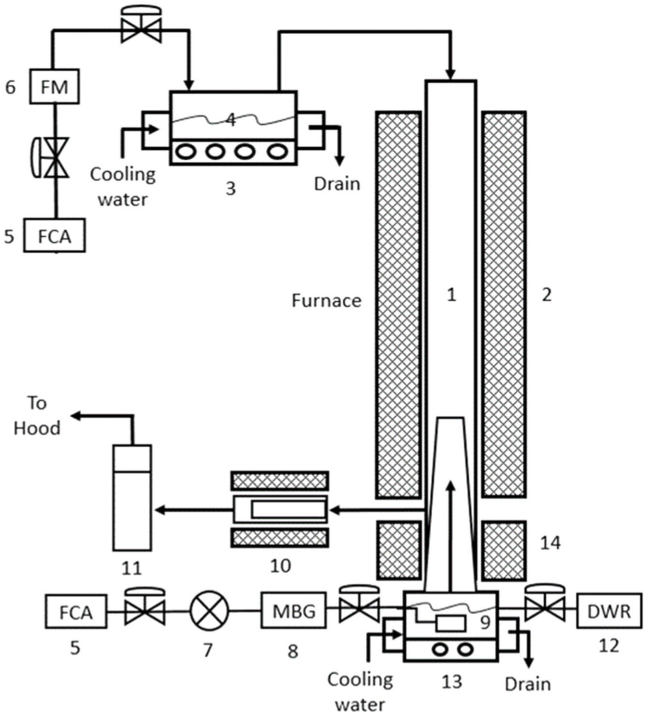

Fig. 1. Schematic diagram of experimental apparatus.

1. Reactor
2. Furnace
3. Ultrasonic atomizer
4. Precursor solution
5. Filtered & compressed air
6. Flow meter
7. Regulator & controller
8. Micro Bubble Generator
9. Microbubble port
10. Filter & collector
11. Gas scrubber
12. Distilled water reservoir
13. Liquid foam generator
14. Calming section

3. Results and Discussion

Fig. 2 shows the crystalline phases of as-prepared SnO_2 and SnO_2:Ga powders determined by XRD with varying the amount of Ga^{3+} (C_{Ga}). In XRD patterns, all the diffraction peaks could be well indexed to the tetragonal structure of SnO_2 based on the standard data file (JCPDS file no. 41-1445), confirming that single crystal phases of SnO_2 and SnO_2:Ga are mainly formed in a one-step process without any other additional process such as calcination, annealing, washing, and drying. Any other considerable characteristic peaks of impurities were not detected. The magnifications of the main peaks around

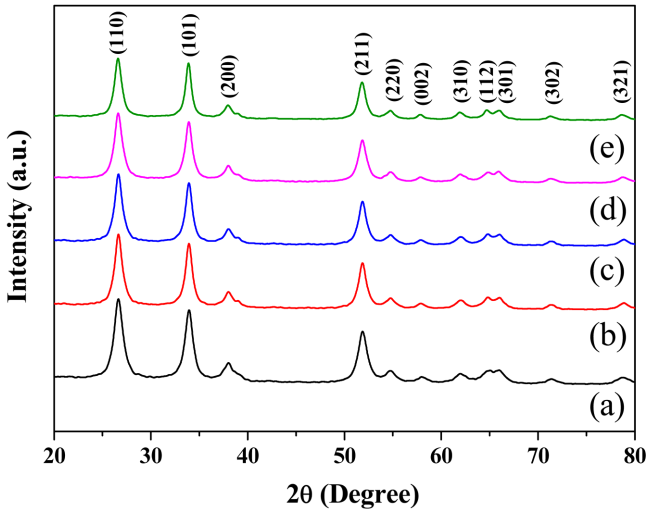

Fig. 2. X-ray diffraction pattern of SnO_2 and SnO_2:Ga powders prepared in the micro drop fluidized reactor (C_{Ga} [at.%]: (a) 0, (b) 1.0, (c) 1.5, (d) 2.0, (e) 3.0).

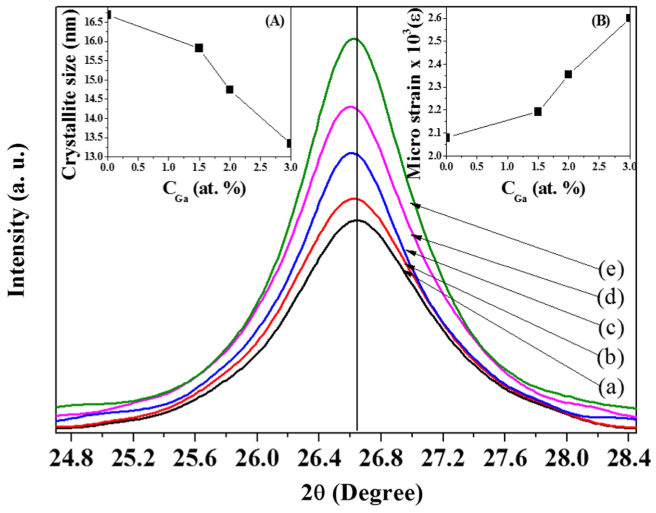

Fig. 3. Magnification of the diffraction peak around 26.7°. The insets of (A) and (B) show the crystallite size and micro strain of SnO_2:Ga with varying C_{Ga}, respectively (C_{Ga} [at.%]: (a) 0, (b) 1.0, (c) 1.5, (d) 2.0, (e) 3.0).

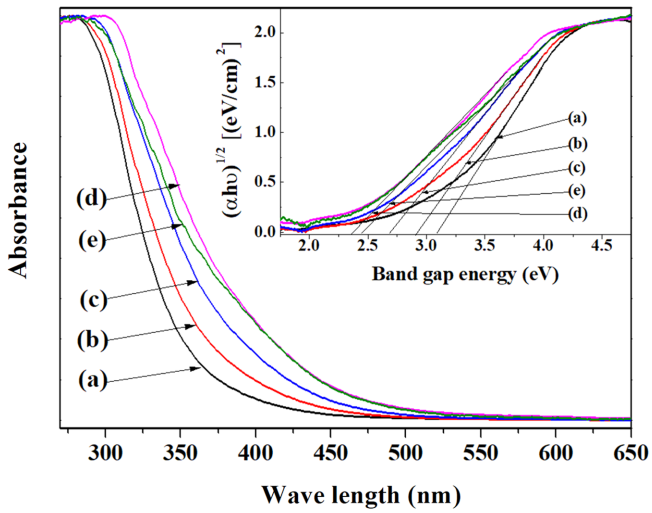

Fig. 4. Diffuse reflectance spectra of SnO_2 and SnO_2:Ga powders prepared in the micro drop fluidized reactor. The inset shows the change of band gap energy with varying C_{Ga} (C_{Ga} [at.%]: (a) 0, (b) 1.0, (c) 1.5, (d) 2.0, (e) 3.0).

26.7° for (110) plane were shifted toward lower angles with varying C_{Ga} (Fig. 3), indicating that the Ga^{3+} ions were doped into the crystal lattice of SnO_2. Since the ionic radius of Ga^{3+} (0.062 nm) is similar to that of Sn^{4+} (0.069 nm), some parts of Sn^{4+} in the crystal lattice of host material were easily substituted by Ga^{3+}[53]. The substitution of Ga^{3+} for Sn^{4+} resulted in a slight distortion of the lattice structure of SnO_2 [18], representing a slight shift of the main peaks toward a lower angle. Note that the shift increased with increasing C_{Ga} up to 2.0 at.%; however, the shift tended to decrease with a further increase in C_{Ga} from 2.0 to 3.0 at%. The inset of Fig. 3(A) shows that the crystallite size of SnO_2:Ga Powders decreased with increasing C_{Ga}, because of the corresponding increase in the number of defects in the crystal lattice [42,54,55]. The crystallite size was calculated by using the Scherrer equation from XRD data.

Fig. 4 shows the diffuse reflectance spectra (DRS) of SnO_2 and SnO_2:Ga at different Ga^{3+} content doped into the SnO_2 lattice. The spectra were transformed to absorbance intensity through the Kubela-Munk method. The doping of Ga^{3+} into SnO_2 extended the absorption band to the longer wavelength, indicating the modification of the band gap structure of SnO_2. In the inset of Fig. 4, the band gap energy of SnO_2:Ga powders, which was estimated from the onset of the absorption of DRS analysis, decreased with increasing Ga^{3+} content up to 2.0 at.% but it increased slightly with a further increase in C_{Ga} from 2.0 to 3.0 at.%, as listed in Table 1. The shifts of spectra pattern to the visible region are associated with the change of electron coordination around the Sn^{4+} ions, resulting in the change of band gap structure. It can be ascribed to the formation of a new energy level of Ga-O between the conduction and valance bands of SnO_2 [42,48-50, 56]. That is, the bandgap energy of SnO_2 powders prepared in the MDFR was 3.09 eV, which is composed of Sn 5s5p conduction band and O 2p valance band. However, the substitution of Ga^{3+} ions for Sn^{4+} ions could lead to the formation of an acceptor level (Ga^{3+} 4s4p) below the conduction band of Sn, which results in the decrease in the bandgap energy.

Fig. 5 shows the field-emission SEM images of as-prepared SnO_2 and SnO_2:Ga powders. The powders were spherical and porous; however, the surface became more wrinkled and furrowed with increasing C_{Ga}. The size of aggregate was in the range of 500 - 600 nm. The change of surface morphology of SnO_2:Ga powders is ascribed to the doping of Ga^{3+} into SnO_2 which induces the formation of partitioned parts at the surface of the powders. The unique partitioned parts can be due to the change of ionic strength and electro-negativity in the lattice of SnO_2 by doping Ga^{3+} ions. The effects of regional breaking of charge homogeneity at the surface of the powders could increase with increasing dopant content [39].

Fig. 6 shows the room - temperature photoluminescence (PL) spectra of as-prepared powders. In Fig. 6, all the samples have a broad visible emission centered at 530~600 nm, due to the vacancies of oxygen and interstitial tin [7,16,17,22,31,32,38]. The intensity of PL spectra becomes weaker with an increase in the content of Ga^{3+}.

Table 1. Crystallite size, bandgap energy and BET surface area of SnO_2:Ga powders

U_C [L/min]	T [°C]	C_{Sn} [mol/L]	U_{MB} [L/min]	$C_{Ga/Sn}$ [at.%]	Crystallite size [nm]	Bandgap energy [eV]	BET surface area [m^2/g]
4.0	800	0.3	0.4	0	16.60	3.09	28.69
4.0	800	0.3	0.4	1.0	16.14	2.91	30.38
4.0	800	0.3	0.4	1.5	15.91	2.64	36.83
4.0	800	0.3	0.4	2.0	14.72	2.36	38.03
4.0	800	0.3	0.4	3.0	13.21	2.44	37.91

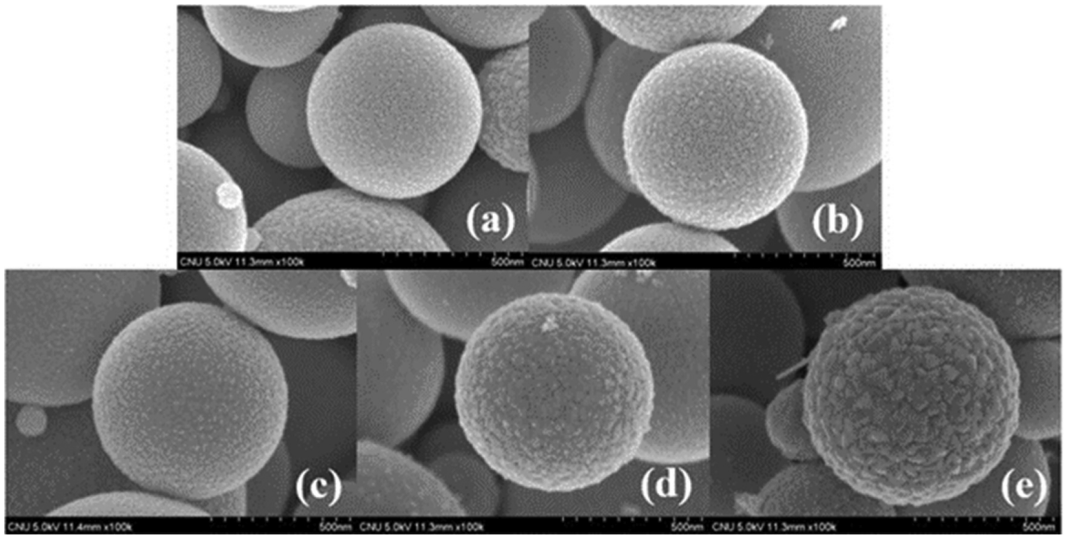

Fig. 5. Field-emission SEM images of SnO_2 and SnO_2:Ga powders prepared in the micro drop fluidized reactor (C_{Ga} [at.%]: (a) 0, (b) 1.0, (c) 1.5, (d)2.0, (e) 3.0).

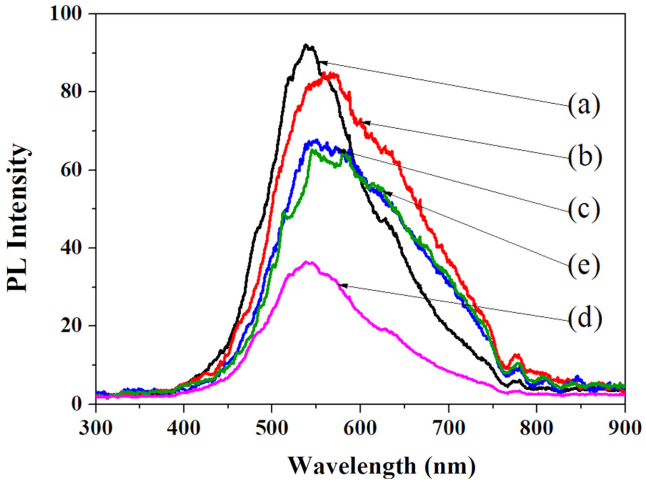

Fig. 6. Room temperature photoluminescence spectra of SnO_2 and SnO_2:Ga powders prepared in the micro drop fluidized reactor (C_{Ga} [at.%]: (a) 0, (b) 1.0, (c) 1.5, (d) 2.0, (e) 3.0).

Similar trends were also observed by doping of Zn, Fe or Ag into SnO_2 lattice prepared by hydrothermal method [31,38]. Since the PL spectra reflect the charge transfer at the surface of the material, the doping of Ga^{3+} into SnO_2 lattice can induce the charge transfer due to vacancies of the oxygen and interfacial tin. The vacancies could lead to the formation of trapped states by forming metastable energy level in the band gap structure, which consequently results in the induction of charge transfer at the surface of host material. The vacancies of oxygen and interfacial tin could increase with increasing the content of Ga^{3+} doped into SnO_2 lattice. Thus, the intensity of PL spectra became weaker with increasing C_{Ga} up to 2.0 at.%. However, the PL intensity tended to increase slightly with a further increase in C_{Ga} from 2.0 to 3.0 at.%. Because, the modified band gap structure of SnO_2 by doping Ga^{3+} ions could be less effective with a further increase in C_{Ga} owing to the recombination of charge carriers [32,38].

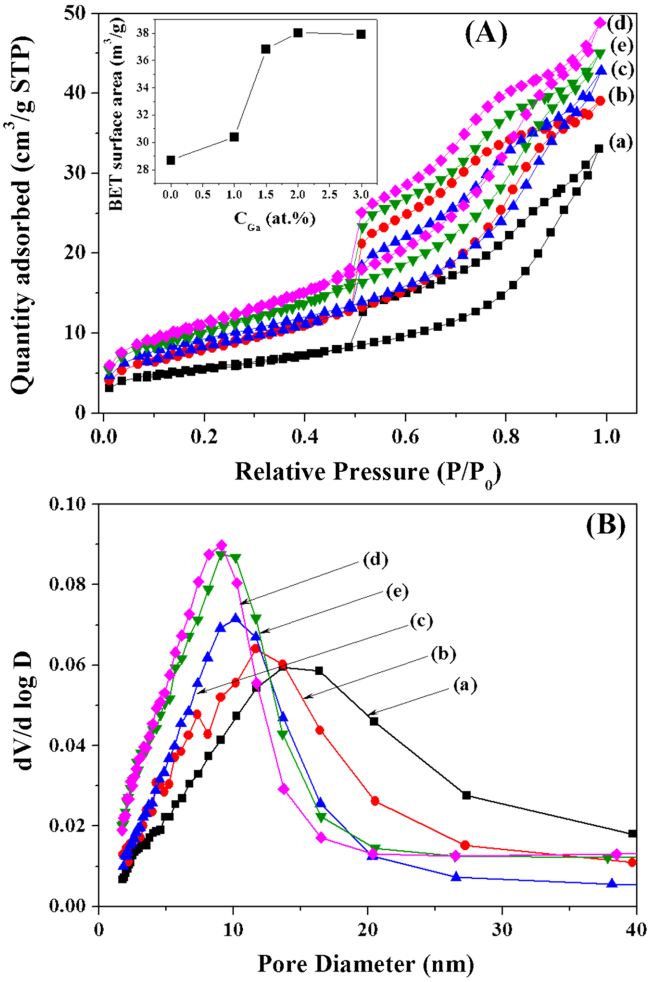

Fig. 7. (A) Nitrogen adsorption isotherms and (B) BJH pore size distribution of SnO_2 and SnO_2:Ga powders prepared in the micro drop fluidized reactor. The inset of (A) shows the BET surface area with varying C_{Ga} (C_{Ga} [at.%]: (a) 0, (b) 1.0, (c) 1.5, (d) 2.0, (e) 3.0).

Fig. 7 shows the nitrogen adsorption isotherms (Fig. 7A) and pore size distribution (Fig. 7B) of SnO_2:Ga powders. All of the isotherms

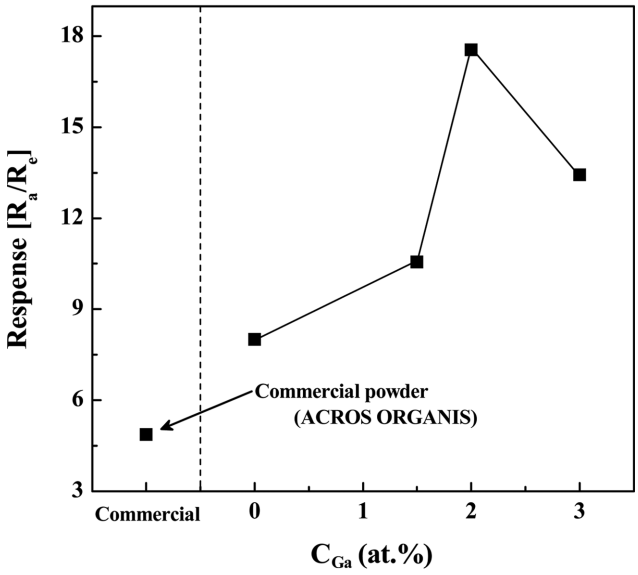

Fig. 8. Effects of C_{Ga} on the response of SnO_2:Ga powders to ethyl alcohol (100 ppm) at 150 °C.

show Type IV hysteresis loops according to the IUPAC classification. The inset of Fig. 7(A) shows that the BET surface area of SnO_2:Ga powders increases with increasing C_{Ga} up to 2.0 at.%, but it decreases slightly at 3.0 at.%, indicating a maximum at 2.0 at.%. The main peaks of pore size distribution are in the range of 8~15 nm, and the distributions tend to shift to the smaller size range with increasing C_{Ga}, showing the smallest pore size distribution at the content of Ga^{3+} is 2.0 at.% (Fig. 7(B)).

Fig. 8 shows the effects of C_{Ga} on the response of SnO_2:Ga samples to ethyl alcohol at 150 °C. The Ra and Re are the resistances in air and ethyl alcohol, respectively. Compared to the commercial powders, the response of SnO_2 powders prepared by MDFR shows higher relative resistance (Ra/Re). In addition, the doping of Ga^{3+} enhances the response intensity, exhibiting a maximum at C_{Ga} is 2.0 at.%, due to the increase in the number as well as strength of active sites [8,14,15,30].

Fig. 9 shows the transient relative response of SnO_2:Ga samples to ethyl alcohol (100 ppm) at 150 C with varying C_{Ga}. The response and recovery times were 5~8 s and 7~10 s, respectively. The response behavior becomes sensitive with increasing C_{Ga} up to 2.0 at.%. Since the electrical resistance stems basically from the charge transfer at the surface of the sensor, the doping of Ga^{3+} ions into SnO_2 lattice resulted in the loss of oxygen and generation of free electrons and holes, so that the extrinsic semiconducting properties could take place at the surface of host materials. The electric resistivity could decrease with increasing oxygen vacancies as well as densities of free electrons and holes at the active sites of the surface, since they are highly sensitive to the external sensing gas [3,17,57- 60]. However, the resistivity could increase with a further increase in C_{Ga}, showing a minimum value at C_{Ga} is 2.0 at.%. This can be because the charge carriers tend to interact with the ionic lattice in SnO_2 with increasing the amount of Ga^{3+} ions. That is, the extra free electrons and oxygen vacancies generated by the doping of Ga^{3+} ions could interact for recombination, which prevents the active sites of SnO_2:Ga from the surface reaction with exterior gas (ethyl alcohol) and thus from the gas sensing [17,38,61-64].

Fig. 10 shows the FT-IR spectrum of as-prepared SnO_2 and SnO_2:Ga powders at different content of Ga^{3+} ions, by which the chemical compositions and bonds were analyzed. Sn-O vibration modes such as Sn-O-Sn and O-Sn-O were observed between 600 and 800 cm^{-1}, indicating that some of metal oxides were bounded more than one oxygen atom [3,15,64-67]. The Sn-OH vibration peak was observed at around 1110 cm^{-1}. The O-H bending vibration peak due to the adsorbed water molecule was observed at 1610 cm^{-1}. Broad band peaks of hydrogen bounded OH group on the surface of SnO_2:Ga were observed between 3300~3650 cm^{-1} [3,7,15,64,68-70]. Note that the distinctive peak indicating the presence of OH group on the surface of SnO_2:Ga powders was most noticeable at C_{Ga} is 2.0 at.%.

Fig. 11 shows the scheme of excitation and separation of electron-hole pairs and possible reaction mechanism of SnO_2:Ga powders with

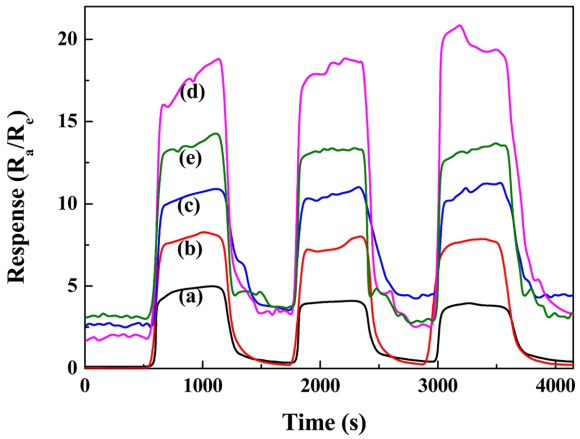

Fig. 9. Transient response of SnO_2:Ga powders to ethyl alcohol (100 ppm) at 150 °C with varying C_{Ga} (C_{Ga} [at.%]: (a) commercial (Acros Organics), (b) 0, (c) 1.5, (d) 2.0, (e) 3.0).

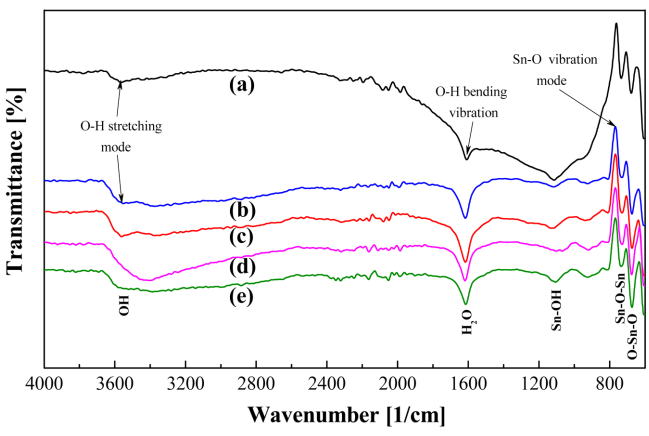

Fig. 10. FT-IR spectra of SnO_2 and SnO_2:Ga powders prepared in the micro drop fluidized reactor (C_{Ga} [at.%]: (a) 0, (b) 1.0, (c) 1.5, (d) 2.0, (e) 3.0).

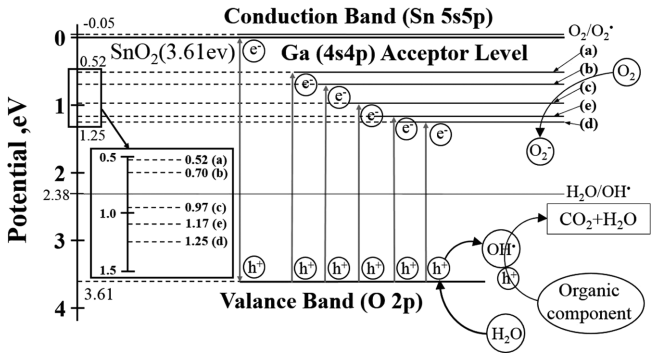

Fig. 11. Scheme of excitation and separation of electrons-holes pairs in the band gap structure and possible reaction mechanism of SnO_2:Ga powders (C_{Ga} [at.%]: (a) 0, (b) 1.0, (c) 1.5, (d) 2.0,(e) 3.0).

varying C_{Ga}. Since the new formed Fermi energy level of SnO_2:Ga hetero structure is lower than that of the bottom of the conduction band of the SnO_2, the excited and separated electrons could be easily transferred to the acceptor level of Ga 4s4p, with remaining holes at the surface of SnO_2 [38,61,70-72]. The adsorbed oxygen associated with the electrons on Ga^{3+}ions could be formed O^{2-}, and the holes could decompose H_2O into OH^- at the surface of SnO_2. Both radicals could capture organic component such as ethyl alcohol, resulting in the surface reaction and thus the sensing. However, the excessive Ga^{3+} ions over a certain value (C_{Ga} is 2.0 at.%) could act as recombination centers of separated electrons and holes owing to the electrostatic attraction between the Ga^{3+}ions and holes, which consequently results in the decrease in the surface activities of SnO_2:Ga hetero structure [28,38,61-63,70-72].

4. Conclusion

Effective tuning of electro-optical properties of nano-structured SnO_2:Ga powders was conducted successfully by employing a micro drop fluidized reactor. The bend gap structure was modified easily and the surface activity of SnO_2:Ga powders was enhanced controllably in a facile one-step process. The amount of dopant (Ga^{3+} ions) to minimize the band gap energy and to maximize the BET surface area as well as charge transfer at the surface of the material was 2.0 at.% within this experimental conditions. The response of as-prepared SnO_2 powders to ethanol vapor was somewhat higher that of commercial powder, and the response became more sensitive with increasing the amount of Ga^{3+} ions doped into SnO_2 up to 2.0 at.%. A possible reaction mechanism was obtained to explain the surface activity of as-prepared SnO_2:Ga powders.

Acknowledgments

This work was supported by the National Research Foundation of Korea (NRF) grant funded by Korea government (NRF-2013R1A1A2059124).

References

1. Wang, H., Fu, F., Zhang, F., Wang, H. E., Kershaw, S. V., Xu, J., Sun, S. G. and Rogach, A. L., "Hydrothermal Synthesis of Hierarchical SnO_2 Micro Spheres for Gas Sensing and Lithium-ion Batteries Applications: Fluoride-mediated Formation of Solid and Hollow Structures," *J. Mater. Chem.,* **22**(5), 2140-2148(2012).
2. Han, Y., Wu, X., Shen, G., Dierre, B., Gong, L., Qu, F., Bando, Y., Sekiguchi, T., Filippo, F. and Golberg D., "Solution Growth and Cathodoluminescence of Novel SnO_2 Core-shell Homogeneous Microspheres," *J. Phys. Chem.*, **114**(18), 8235-8240(2010).
3. Liu, Y., Jiao, Y., Zhang, Z., Qu, F., Umar, A. and Wu, X., "Hierarchical SnO_2 Nanostructures Made of Intermingled Ultrathin Nanosheets for Environmental Remediation, Smart Gas Sensor, and Supercapacitor Applications," *ACS Appl. Mater. Interfaces*, **6**(3), 2174-2184(2014).
4. Liu, B., Cheng, C. W., Chen, R., Shen, Z. X., Fan, H. J. and Sun, H. D., "Fine Structure of Ultraviolet Photoluminescence of tin Oxide Nanowires," *J. Phys. Chem. C*, **114**(8), 3407-3410(2010).
5. Gu, F., Wang, S. F., Lü, M. K., Zhou, G. J., Xu, D. and Yuan, D. R., "Photoluminescence Properties of SnO_2 Nanoparticles Synthesized by Sol-gel Method," *J. Phys. Chem. B*, **108**(24), 8119-8123(2004).
6. Du, J., He, S., Zhao, R., Chen, S., Guo, T. and Wang, H., "Facile Self-assembly of SnO_2 Nanospheres for Volatile Amine Gas Sensing," *Mater. Lett.*, **186**, 318-321(2017).
7. Bonu, V., Das, A., Prasad, A. K., Krishna, N. G., Dhara, S. and Tyagi, A. K., "Influence of in-plane and Bridging Oxygen Vacancies of SnO_2 Nanostructures on CH_4 Sensing at Low Operating Temperatures," *Appl. Phys. Lett.*, **105**, 243102(2014).
8. Wang, L., Wang, S., Wang, Y., Zhang, H., Kang, Y. and Huang, W., "Synthesis of Hierarchical SnO_2 Nanostructures Assembled with Nanosheets and Their Improved Gas Sensing Properties," *Sensors Actuators B.*, **188**, 85-93(2013).
9. Hyodo, T., Sasahara, K., Shimizu, Y. and Egashira, M., "Preparation of Macroporous SnO_2 Films Using PMMA Microspheres and Their Sensing Properties to NOx and H_2," *Sensors Actuators B*, **106**, 580-590(2005).
10. Snaith, H. J. and Ducati, C., "SnO_2-Based Dye-Sensitized Hybrid Solar Cells Exhibiting Near Unity Absorbed Photon-to-Electron Conversion Efficiency," *Nano Lett.*, **10**, 1259-1265(2010).
11. Dai, S. and Yao, Z., "Synthesis of Flower-like SnO_2 Single Crystals and Its Enhanced Photocatalytic Activity," *Appl. Surf. Sci.*, **258**, 5703-5706(2012).
12. Guo, J., Zhang, J., Ju, D., Xu, H. and Cao, B., "Three-dimensional SnO_2 Microstructures Assembled by Porous Nanosheets and Their Superior Performance for Gas Sensing," *App. Surf. Sci.*, **258**, 5703-5706(2013).
13. Bhattacharjee, A. and Ahmaruzzaman, M., "Facile Synthesis of SnO_2 Quantum Dots and Its Photocatalytic Activity in the Degradation of Eosin Y Dye: A Green Approach," *Mater. Lett.*, **139**, 418-421(2014).
14. Guan, Y., Wang, D., Zhou, X., Sun, P., Wang, H., Ma, J. and Lu, G., "Hydrothermal Preparation and Gas Sensing Properties of Zn-doped SnO_2 Hierarchical Architectures," *Sensors Actuators B*, **191**, 45-52(2014).
15. Ben, W., Othmen, H., Sdiri, N., Elhouichet, H. and Férid, M.,

"Study of Charge Transport in Fe-doped SnO_2 Nanoparticles Prepared by Hydrothermal Method," *Mater. Sci. Semiconductor Processing*, **52**, 46-54(2016).
16. Reddy, P. V., Reddy, S. V. and Reddy, B. S., "Synthesis and Properties of (Fe, Al) Co-Doped SnO_2 Nanoparticles," *Mater. Today Proceedings*, **3**, 1752-1761(2016).
17. Xu, X., Sun, J., Zhang, H., Wang, Z., Dong, B., Jiang, T., Wang, W., Li, Z. and Wang, C., "Effects of Al Doping on SnO_2 Nanofibers in Hydrogen Sensor," *Sensors Actuators B*, **160**, 858-863 (2011).
18. Ahmed, S. F., Ghosh, P. K., Khan, S., Mitra, M. K. and Chattopadhyay, K. K., "Low-macroscopic Field Emission from Nano Crystalline Al Doped SnO_2 Thin Films Synthesized by Sol-gel Technique," *Appl. Phys. A*, **86**, 139-143(2007).
19. Fang, L. M., Zu, X. T., Li, Z. J., Zhu, S., Liu, C. M., Zhou, W. L. and Wang, L. M., "Synthesis and Characteristics of Fe^3-doped SnO_2 Nanoparticles via Sol-gel-calcination or Sol-gel-hydrothermal Route," *J. Alloys Compd.*, **454**, 261-267(2008).
20. Nomura, K., Okabayashi, J., Okamura, K. and Yamada, Y., "Magnetic Properties of Fe and Co codoped SnO_2 Prepared by Sol-gel Method," *Cit. J. Appl. Phys.*, **110**, 83901(2011).
21. Huang, Z., Gao, H., Wang, Q., Zhao, Y. and Li, G., "Fabrication of Amorphous SnO_2@C Nanofibers as Anode for Lithium-ion Batteries," *Mater. Lett.*, **186**, 231-234(2017).
22. Huang, H., Tian, S., Xu, J., Xie, Z., Zeng, D., Chen, D. and Shen, G., "Needle-like Zn-doped SnO_2 Nano Rods with Enhanced Photocatalytic and Gas Sensing Properties," *Nanotechnology*, **23**, 105502-105509(2012).
23. Li, Z., Zhou, Y., Yu, T., Liu, J. and Zou, Z., "Unique Zn-doped SnO_2 Nano-echinus with Excellent Electron Transport and Light Harvesting Properties as Photo Anode Materials for High Performance Dye-sensitized Solar Cell," *Cryst Eng Comm*, **14**, 6462-6468(2012).
24. Mondal, B., Basumatari, B., Das, J., Roychaudhury, C., Saha, H. and Mukherjee, N., "ZnO-SnO_2 Based Composite Type Gas Sensor for Selective Hydrogen Sensing," *Sensors Actuators B.*, **194**, 389-396(2014).
25. Tang, W., Wang, J., Yao, P. and Li, X., "Hollow Hierarchical SnO_2-ZnO Composite Nanofibers with Heterostructure Based on Electrospinning Method for Detecting Methanol," *Sensors Actuators B*, **192**, 543-549(2014).
26. Wang, H., Dou, K., Teoh, W. Y., Zhan, Y., Hung, T. F., Zhang, F., Xu, J., Zhang, R. and Rogach, A. L., "Engineering of Facets, Band Structure, and Gas-sensing Properties of Hierarchical Sn^{2+} Doped SnO_2 Nano Structures," *Adv. Funct. Mater.*, **23**(38), 4847-4853(2013).
27. Lei, M., Hu, Q. R., Wang, S. L. and Tang, W. H., "Structural and Optical Properties of Al-doped SnO_2 Nanowires," *Mater. Lett.*, **64**, 19-21(2009).
28. Cui, S., Wen, Z., Mattson, E. C., Mao, S., Chang, J., Weinert, M., Hirschmugl, C. J., Gajdardziska-Josifovska, M. and Chen, J., "Indium-doped SnO_2 Nanoparticle-graphene Nanohybrids: Simple One-pot Synthesis and Their Selective Detection of NO_2," *J. Mater. Chem. A*, **1**(14), 4462-4467(2013).
29. Nilavazhagan, S. and Muthukumaran, S., "Investigation of Optical and Structural Properties of Fe, Cu co-doped SnO_2 Nanoparticles," *Superlattices Microstruct.*, **83**, 507-520(2015).
30. Wang, W., Tian, Y., Li, X., Wang, X., He, H., Xu, Y. and He, C., "Enhanced Ethanol Sensing Properties of Zn-doped SnO_2 Porous Hollow Microspheres," *Appl. Surf. Sci.*, **261**, 890-895(2012).
31. Mazloom, J., Ghodsi, F. E. and Golmojdeh, H., "Synthesis and Characterization of Vanadium Doped SnO_2 Diluted Magnetic Semiconductor Nanoparticles with Enhanced Photocatalytic Activities," *J. Alloys Compd.*, **639**, 393-399(2015).
32. Niu, M., Huang, F., Cui, L., Huang, P., Yu, Y. and Wang, Y., "Hydrothermal Synthesis, Structural Characteristics, and Enhanced Photocatalysis of SnO_2/α-Fe_2O_3 Semiconductor Nanoheterostructures," *Nano*, **4**, 681-688(2010).
33. Li, Z., Li, X., Zhang, X. and Qian, Y., "Hydrothermal Synthesis and Characterization of Novel Flower-like Zinc-doped SnO_2 Nanocrystals," *J. Cryst. Growth*, **291**, 258-261(2006).
34. Kaur, J., Shah, J., Kotnala, R. K. and Verma, K. C., "Raman Spectra, Photoluminescence and Ferromagnetism of Pure, Co and Fe Doped SnO_2 Nanoparticles," *Ceramics Int'l.*, **38**, 5563-5570(2012).
35. Manikandan, D. and Murugan, R., "Room Temperature Dilute Magnetism in Nanoscale Co and Zn co-doped SnO_2," *Superlattices Microstruct.*, **89**, 7-14(2016).
36. Mohagheghi, M. B. and Saremi, M. S., "Semiconductor Science and Technology Electrical, Optical and Structural Properties of Li-doped SnO_2 Transparent Conducting Films Deposited by the Spray Pyrolysis Technique: A Carrier-type Conversion Study," *Semicond. Sci. Technol.*, **19**, 764-769(2004).
37. Cheng, G., Wu, K., Zhao, P., Cheng, Y., He, X. and Huang, K., "Solvothermal Controlled Growth of Zn-doped SnO_2 Branched Nanorod Clusters," *J. Cryst. Growth*, **309**(1), 53-59(2007).
38. Wang, X., Fan, H. and Ren, P., "Self-assemble Flower-like SnO_2/Ag Heterostructures: Correlation Among Composition, Structure and Photocatalytic Activity," *Colloids Surfaces A Physicochem. Eng. Asp.*, **419**, 140-146(2013).
39. Gurakar, S., Serin, T. and Serin, N., "Electrical And Microstructural Properties Of (Cu, Al, In)-doped SnO_2 Films Deposited By Spray Pyrolysis," *Adv. Mater. Lett.*, **5**(6), 309-314(2014).
40. Kim, J. H., Choi, C., Kim, H. Y., Kang, Y. and Park, Y. K., "Preparation of Mono-dispersed Mixed Metal Oxide Micro Hollow Spheres by Homogeneous Precipitation in a Micro Precipitator," *Powder Technol.,* **153**, 166-175(2005).
41. Kang, Y., Lee, C. K., Kang, G. M., Lim, D. H. and Yoo, D. J., "Aluminum ion and Lithium ion and Zinc ion co-doped Tin Oxide and Method for Continuous Synthesis the Same," Korea Patent No. 10-1757424(2017).
42. Kang, H. W., Lim, S. N. and Park, S. B., "Effect of Tri-doping on H_2 Evolution Under Visible Light Irradiation on $SrTiO_3$:Ni/Ta/La Prepared by Spray Pyrolysis from Polymeric Precursor," *Int. J. Hydrogen Energy*, **37**(14), 10539-10548(2012).
43. Park, G. D., Cho, J. S. and Kang, Y. C., "Multiphase and Double-Layer $NiFe_2O_4$@NiO-Hollow-Nanosphere-Decorated Reduced Graphene Oxide Composite Powders Prepared by Spray Pyrolysis Applying Nanoscale Kirkendall Diffusion," *ACS Appl. Mater. Interfaces*, **7**, 16842-16849(2015).
44. 44. Ko, Y. N., Park, S. B., Jung, K. Y. and Kang, Y. C., "One-Pot Facile Synthesis of Ant-Cave-Structured Metal Oxide-Carbon Microballs by Continuous Process for Use as Anode Materials in Li-Ion Batteries," *Nano Lett.*, **13**, 5462-5466(2013).
45. Okuyama, K. and Lenggoro, W., "Preparation of Nanoparticles

via Spray Route," *Chem. Eng. Sci.*, **58**(3-6), 537-547(2003).
46. Hieda, K., Hyodo, T., Shimizu, Y. and Egashira, M., "Preparation of Porous Tin Dioxide Powder by Ultrasonic Spray Pyrolysis and Their Application to Sensor Materials," *Sensors Actuators B*, **133**, 144-150(2008).
47. Kim, W. S., Kang, Y. and Kim, Y. C., "Synthesis of Manganese Hydrogen Phosphate Hydrate by Controlled Double-jet Precipitation," *Korean Chem. Eng. Res.*, **19**, 66-72(2008).
48. Kang, Y., Lee, C. K., Kang, G. M., Lim, D. H. and Yoo, D. J., "Aluminum ion and Zinc ion Doped Tin Oxide and Method for Continuous Synthesis the Same," Korea Patent No. 10-1765448(2017).
49. Yoo, D. J., Lim, D. H., Kang, Y., Lee, C. G. and Kang, G. M., "Opto-electrical Properties of ZnO:Al Powders Prepared in a Micro Drop Fluidized Reactor," *Mater. Chem. Phys.*, **183**, 398-404(2016).
50. Yoo, D. J., Lim, D. H., Kang, Y., Lee, C. G. and Kang, G. M., "Optical Properties of Nano–Structured ZnO:Sn Powders Prepared in a Micro Drop Fluidized Reactor," *J. Chem. Eng. Japan*, **50**(1), 21-25(2017).
51. Yang, S. W., Lim, D. H., Yoo, D. J., Kang, Y., Lee, C. G. and Kang, G. M., "Opto-magnetic Properties of Nano-structured MgO:Al Powders Prepared in a Micro Drop Fluidized Reactor," *Adv. Powder Technol.*, **29**(3), 499-505(2018).
52. Cheng, B., Russell, J. M., Shi, W., Zhang, L. and Samulski, E. T., "Large-Scale, Solution-Phase Growth of Single-Crystalline SnO_2 Nanorods," *J. Am. Chem. Soc.*, **126**, 5972-5973(2004).
53. Shannon, R. D., "Revised Effective Ionic Radii and Systematic Studies of Interatomie Distances in Halides and Chaleogenides," *Acta. Cryst. A*, **32**, 751-767(1976).
54. Jia, A., Liang, X., Su, Z., Zhu, T. and Liu, S., "Synthesis and the Effect of Calcination Temperature on the Physical-chemical Properties and Photocatalytic Activities of Ni, La Codoped $SrTiO_3$," *J. Hazard. Mater.*, **178**(1-3), 233-242(2010).
55. Li, F., Yu, K., Lou, L. L., Su, Z. and Liu, S., "Theoretical and Experimental Study of La/Ni co-doped $SrTiO_3$ Photocatalyst," *Mater. Sci. Eng. B*, **172**(2), 136-141(2010).
56. Liu, H., Cao, W., Su, Y., Wang, Y. and Wang, X., "Synthesis, Characterization and Photocatalytic Performance of Novel Visible-light-induced Ag/BiOI," *Applied Catal. B: Environ.*, **111**, 271-279(2011).
57. Yin X. T. and Guo, X. M., "Selectivity and Sensitivity of Pd-loaded and Fe-doped SnO_2 Sensor for CO Detection," *Sensors Actuators B*, **200**, 213-218(2014).
58. Rani, S., Roy, S. C. and Bhatnagar, M. C., "Effect of Fe Doping on the Gas Sensing Properties of Nano-crystalline SnO_2 Thin Films," *Sensors Actuators B*, **122**(1), 204-210(2007).
59. Fukui, K. and Nakane, M., "CO Gas Sensor Based on Au-La_2O_3 Loaded SnO_2 Ceramic," *Sensors Actuators B*, **25**(1-3), 486-490 (1995).
60. Zhang, T., Liu, L., Qi, Q., Li, S. and Lu, G., "Development of Microstructure In/Pd-doped SnO_2 Sensor for Low-level CO Detection," *Sensors Actuators B*, **139**(2), 287-291(2009).
61. Liu, Z., Sun, D. D., Guo, P. and Leckie, J. O., "An Efficient Bicomponent TiO_2 /SnO_2 Nanofiber Photocatalyst Fabricated by Electrospinning with a Side-by-Side Dual Spinneret Method," *Nano Lett.*, **7**(4), 1081-1085(2007).
62. Kumar, P. S. S., Manivel, A. and Anandan, S., "Synthesis of Ag-ZnO Nanoparticles for Enhanced Photocatalytic Degradation of Acid Red 88 in Aqueous Environment," *Water Sci. Technol.*, **59**(7), 1423-1430(2009).
63. Wang, H., Niu, J., Long, X. and He, Y., "Sonophotocatalytic Degradation of Methyl Orange by Nano-sized Ag/TiO_2 Particles in Aqueous Solutions," *Ultrason. Sonochem.*, **15**(4), 386-392(2008).
64. Reddy, C. V., Babu, B. and Shim, J., "Synthesis of Cr-doped SnO_2 Quantum Dots and Its Enhanced Photocatalytic Activity," *Mater. Sci. Eng. B*, **223**, 131-142(2017).
65. Baranauskas, V., Fontana, M., Guo, Z. J., Ceragioli, H. J. and Peterlevitz, A. C., "Field-emission Properties of Nanocrystalline Tin Oxide Films," *Sensors Actuators B*, **107**, 474-478(2005).
66. Gnanam S. and Rajendran, V., "Preparation of Cd-doped SnO_2 Nanoparticles by Sol-gel Route and Their Optical Properties," *J. Sol-Gel Sci. Technol.*, **56**, 128-133(2010).
67. Long, D. A., "Infrared and Raman Characteristic Group Frequencies," G. Socrates (ed.), 3rd ed. Wiley, NY, (2001).
68. Farahani, H., Wagiran, R. and Hamidon, M. N., "Humidity Sensors Principle, Mechanism, and Fabrication Technologies: A Comprehensive Review," *Sensors*, **14**(5), 7881-939(2014).
69. Bonu, V., Das, A., Amirthapandian, S., Dhara, S. and Tyagi, A. K., "Photoluminescence of Oxygen Vacancies and Hydroxyl Group Surface Functionalized SnO_2 Nanoparticles," *Phys. Chem. Chem. Phys.*, **17**, 9774-9801(2015).
70. Chikhale, L. P., Patil, J. Y., Rajgure, A. V., Shaikh, F. I., Mulla, I. S. and Suryavanshi, S. S., "Co-precipitation Synthesis of Nanocrystalline SnO_2: Effect of Fe Doping on Structural, Morphological and Ethanol Vapor Response Properties," *Measurement*, **57**, 46-52(2014).
71. Xiong, Y., Zhang, G., Zhang, S., Zeng, D. and Xie, C., "Tin Oxide Thick Film by Doping Rare Earth for Detecting Traces of CO_2: Operating in Oxygen-free Atmosphere," *Mater. Res. Bull.*, **52**, 56-64(2014).
72. Vamathevan, V., Amal, R., Beydoun, D., Low, G. and McEvoy, S., "Photocatalytic Oxidation of Organics in Water Using Pure and Silver-modified Titanium Dioxide Particles," *J. Photochem. Photobiol.*, **148**(1-3), 233-245(2002).